J Mol Model (2012) 18:2577–2588
DOI 10.1007/s00894-011-1271-5

ORIGINAL PAPER

# Conformational and stereoelectronic investigation of tryptamine. An AIM/NBO study

**Rosana M. Lobayan · María C. Pérez Schmit · Alicia H. Jubert · Arturo Vitale**

Received: 25 June 2011 / Accepted: 5 October 2011 / Published online: 11 November 2011


**Abstract** Due to the free radical scavenger properties of Tryptamine (TRA), as well as of others indole derivatives, it is in our interest to explore deeply the stereoelectronic aspects that would be relevant in their stabilization and antioxidant activity. In this work the conformational space of TRA was scanned using molecular dynamics complemented with functional density calculations at B3LYP/6-31+G** level. Twenty one conformers of lowest energy were obtained, their electronic distributions were analyzed at a higher calculation level, thus improving the basis set (B3LYP/6-311++G**). A topological study based on Bader's theory (AIM: atoms in molecules) and natural bond orbital (NBO) framework was performed. The study was enriched by a deep analysis of maps of molecular electrostatic potential (MEP) through a coordinated NBO/AIM analysis. The conformational preferences were explained by hyperconjugative interactions, which were revealed by NBO data. Because radical scavenging by indolic compounds is strongly modulated by their functional residues our study was related to similar analysis done previously on Indole and 1*H*-indole-3-acetic acid (IAA). Therefore, the conformational space of TRA was studied from a new perspective focusing on a deep analysis of the geometric and electronic properties of TRA conformers. The changes of the electronic distribution introduced by the substituent and the conformational flexibility of the side chain were addressed. The results reported contribute to the understanding of the structure, stability and reactivity of TRA and others indole derivatives.

**Keywords** Antioxidants · Atoms in molecules theory · Density functional theory · Molecular electrostatic potential · Natural bond orbital analysis · Tryptamine

Rosana M. Lobayan and María C. Pérez Schmit contributed equally to this work.

**Electronic supplementary material** The online version of this article (doi:10.1007/s00894-011-1271-5) contains supplementary material, which is available to authorized users.

R. M. Lobayan (✉) · M. C. Pérez Schmit
Facultad de Ingeniería, Universidad de la Cuenca del Plata,
Lavalle 50,
3400 Corrientes, Argentina
e-mail: rlobayan@ucp.edu.ar

A. H. Jubert
CEQUINOR Facultad de Ciencias Exactas y Facultad de Ingeniería, Universidad Nacional de La Plata,
C:C: 962,
1900 La Plata, Argentina

A. Vitale
PRALIB (UBA, CONICET), Facultad de Farmacia y Bioquímica,
Universidad de Buenos Aires,
Junín 956,
C1113AAD Buenos Aires, Argentina

## Introduction

The TRA (3-[2-aminoethyl]indole) is an important neurotransmitter, which bears a close structural and chemical similarity to the neurotransmitter serotonin (5-hydroxytryptamine) and to melatonin (5-methoxy- *N*-acetyltryptamine), which plays a key role in the daily behavioral and physiological states of humans. In all three molecules, the conformational flexibility of the ethylamine or *N*-acetyl-ethylamine side chain plays an important role in its binding to receptor sites.

Furthermore TRA, as others indolic compounds are very efficient antioxidants, protecting both lipids and proteins from peroxidation, and it is known that the indole structure influences their antioxidant efficacy in biological systems [1–4]. Radical scavenging by indolic compounds is strongly modulated by their functional residues. All indolamines have

an heteroaromatic ring system of high electroreactivity and they only differ in the functional group in their side chain. These substituents determine to a great extent the reactivity, potency, and efficiency of radical scavenging activity [5]. There are two possible reaction pathways through which indolic compounds scavenge free radicals: (1) rapid donation of the hydrogen atom to a radical form, forming a new radical, more stable than the initial one (mechanism leading to the direct N—H bond breaking) and (2) the chain-breaking mechanism, by which the primary antioxidant donates an electron to the free radical present in the system (e.g., lipid or some other radical), leading to indirect H abstraction. In both mechanisms the N—H bond of the indole ring is the initiator site for free radical scavenging activity.

There is a wide availability of experimental data on the conformers of TRA in the gas phase [6–14]. A variety of spectroscopic techniques combined with supersonic expansion, were employed in order to obtain information on its conformational flexibility. An extensive set of studies of the ultraviolet spectroscopy of jet cooled tryptamine and other tryptophan derivatives were carried out in the past identifying a total of seven conformers [7–11]. Then, experimental studies with resonant ion-dip infrared and UV–UV hole burning spectroscopies were combined with density functional theory (DFT) calculations and nine conformers were described theoretically [12, 13]. Nowadays the conformational landscape of TRA continues to be investigated extensively in several electronic states using a variety of experimental and theoretical methods [14]. To date only seven different conformers of TRA have been identified and characterized experimentally.

Due to the free radical scavenger and antioxidant properties of indole derivatives, particularly of TRA, it is of paramount importance to explore deeply the stereoelectronic aspects that would be relevant in their stabilization and antioxidant activity. In a previous paper we studied the conformational space of 1*H*-indole-3-acetic acid (IAA). We explained the stability order of the conformers, identifying and characterizing intramolecular hydrogen bonding interactions and studying geometrical and topological aspects introduced by the substituent at position 3 [15]. These results were very useful in the interpretation of Raman and infrared spectra of the IAA dimer in solid state [16]. In order to relate the effects introduced by the different substituents on the scavenging capacity of indole ring, some results from our previous work [15] will be used in this paper.

The aim of the present paper is to perform a study of the conformational space of TRA from a new perspective. We focused on the analysis of the geometric and electronic properties of TRA conformers and how the substituents and the conformational flexibility of the side chain introduce electronic changes in the molecule.

The conformational space of TRA was scanned using molecular dynamics (MD) calculations and density functional calculations to optimize the geometry of the lowest-energy conformers as obtained in the simulations. A rigorous approach based on Bader´s atoms in molecules (AIM) theory to detect and characterize hydrogen bond interactions [17, 18], together with natural bond orbital (NBO) analysis were used [19]. Molecular electrostatic potentials (MEPs) were obtained and fully analyzed in light of AIM and NBO results.

## Computational details

The study of conformational space was performed by MD calculations using a module of the HyperChem package [20]. Several simulations were carried out with the aid of the MM+force field. The starting geometry was heated from 0 to 800 K in 0.1 ps.

The system temperature was then kept constant by coupling the system to a thermal bath with a coupling parameter (bath relaxation time) of 0.5 ps. After an equilibration period of 10 ps, a 500 ps-long simulation was carried out saving the molecular cartesian coordinates every 10 ps. The time step for the simulations was 0.5 fs. The resulting geometries were then optimized to an energy gradient less than 0.01 kcal $mol^{-1}$ $Å^{-1}$ at semiempirical level (AM1). The lowest-energy conformers of the molecules, obtained according to the above methodology were further studied by the density functional theory as implemented by the Gaussian 03 package [21]. Geometry optimizations were performed using the Becke three parameter hybrid functional [22] with the Lee-Yang-Parr correlation functional [23], a combination that gives rise to the well known B3LYP method. For all atoms a 6-31+G** basis set was used. All calculations were performed in gas phase with the purpose of obtaining the intrinsic properties of indole derivatives free of solvent effects.

MEPs were obtained in the van der Waals molecule surfaces using the Gaussian 03 software, and were further visualized using the MOLEKEL 4.0 program [24].

The topological analysis and evaluation of local properties were performed with modules of the AIMPAC package [25], using wave functions calculated at the B3LYP level and the improved 6-311++G** basis set. An NBO analysis at the same level was performed [19].

## Results and discussion

The backbone of TRA consists of a heteroaromatic planar indole ring and an aminoethyl side chain (at position 3) which can adopt several distinct orientations with respect to the ring defined by three dihedral angles ($\delta_1$:$C_2$—$C_3$—$C_8$—$C_9$, $\delta_2$: $C_3$—$C_8$—$C_9$—$N_{10}$, $\delta_3$:$C_8$—$C_9$—$N_{10}$—$H_a$) (Fig. 1). Varia-

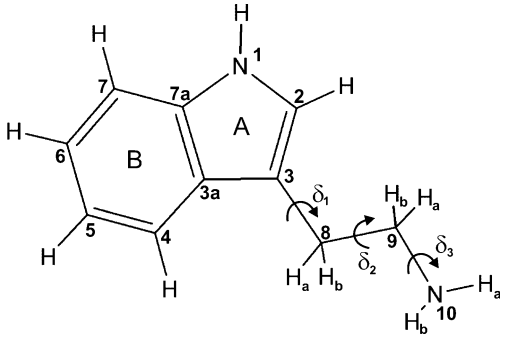


**Fig. 1** Heteroaromatic planar indole ring and an aminoethyl side chain of TRA backbone. Dihedral angles ($\delta_1$: $C_2$—$C_3$—$C_8$—$C_9$, $\delta_2$: $C_3$—$C_8$—$C_9$—$N_{10}$, $\delta_3$: $C_8$—$C_9$—$N_{10}$—$H_a$) defines distinct orientations of aminoethyl side chain with respect to the ring

tions can give rise to several different conformers. Through the study of the conformational space in vacuum we found 21 lowest energy conformers with $C_1$ symmetry, which in stability order were: a) $A^+G^-G^+/A^-G^+G^-$, b) $A^+G^-G^-/A^-G^+G^+$, c) $A^+TG^-/A^-TG^+$, d) $A^+G^+T/A^-G^-T$, e) $A^+TG^+/A^-TG^-$, f) $A^+TT/A^-TT$, g) $A^+G^+G^-/A^-G^-G^+$, h) $CTG^-$, i) $CG^-T/CG^+T$, j) $CTG^+$, k) CTT and l) $A^+G^+G^+/A^-G^-G^-$ (see Fig. 2), according to a previous work [15]. They were named according to IUPAC recommendations, and their existences were confirmed by the absence of imaginary frequencies in the vibrational analysis. Nine pairs of them account for structures of the same energy. They differ in the orientation of the aminoethyl group with respect to the plane of the indole ring: one of them with the aminoethyl moiety upward oriented, *Re*-face, and the other isomer having the aminoethyl moiety downward oriented, *Si*-face. Each pair shows torsion angles of opposite sign. In Table 1 relevant internal coordinates of lowest energy conformers of *Re* isomers of TRA are shown. Due to the similarity of the corresponding electronic distribution we will study only one conformer of each pair, selecting the conformers in which the aminoethyl moiety is upward oriented (*Re* isomers).

At room temperature (298.15 K), the predicted populations for the conformers, taking into account the DFT calculated energies with 6-31+G** basis set, were: 25.70%, 17.36%, 10.32%, 10.29%, 8.13%, 8.07%, 6.58%, 4.18%, 3.97%, 2.53%, 2.53% and 0.35% for $A^+G^-G^-$, $A^+TG^-$, $A^+G^+T$, $A^+TG^+$, $A^+TT$, $A^+G^+G^-$, $CTG^-$, $CG^-T$, $CTG^+$, CTT, and $A^+G^+G^+$, respectively. Experimentally the first seven conformers were observed, and our results agree very well to the experimentally suggested energy ordering [6]. We described also four conformers unobserved experimentally which showed a relative population less than 6%.

## Topology of the electronic charge density function

AIM theory is based on the analysis of critical points (CPs) of the molecular charge density, ρ. At these points, the gradient of the electronic density, ∇ρ, is null, and it is characterized by the three eigenvalues, $\lambda_i$ (i=1, 2, 3), of the $\nabla^2\rho$ Hessian matrix. The CPs are named and classified as (r, s) according to their rank, r (number of non-zero eigenvalues), and signature, s (the three eigenvalues algebraic sum).

Several properties evaluated at the bond CP (BCP) (a (3,-1) CP) constitute powerful tools to classify a given chemical structure [17].

The most significant topological local properties at BCPs for $A^+G^-G^+$ conformer are shown in supplementary material: the electron charge density at BCP ($\rho_b$), the Laplacian of the electron charge density ($\nabla^2\rho_b$), the three eigenvalues of the Hessian matrix ($\lambda_1$, $\lambda_2$ and $\lambda_3$), the ellipticity (ε), the relationship between perpendicular and parallel curvatures ($|\lambda_1|/\lambda_3$), and the kinetic energy density per charge unit ($G_b/\rho_b$), for all chemical bonds of the lowest energy conformers obtained (Tables S1a to S1l).

All BCPs of TRA were characterized by large $\rho_b$ values, significant and less than zero $\nabla^2\rho_b$ values, $|\lambda_1|/\lambda_3>1$ and $G_b/\rho_b<1$, which means that negative curvatures predominate and electron charge is locally concentrated within the interatomic region, thus leading to interaction characteristics of covalent bonds.

Table 2 summarizes the changes in geometric parameters and topological properties introduced in the indole ring when it was substitued at position 3 with acetyl (IAA) and aminoethyl (TRA) moieties. The percentage values take into account the averaged differences of the values from eight conformers (six of them *Si-face*) of IAA and 12 conformers (nine of them *Si-face*) of TRA with respect to Indole, calculated from

$$\%\Delta x_{IAA,TRA} = \frac{x(IAA,TRA) - x(Indole)}{x(Indole)} \times 100. \qquad (1)$$

It was noted that the two rings (benzenic as well as pyrrolic) showed changes in bond lengths and topological properties.

In IAA as in TRA, ring A showed higher changes than ring B. In IAA was observed a shortening of the $N_1$—$C_{7a}$, $N_1$—$C_2$ and $C_{3a}$—$C_{7a}$ bonds and a lengthening of the $C_2$—$C_3$ and $C_3$—$C_{3a}$ bonds. Consequently an increase of $\rho_b$ was found in BCPs of the $N_1$—$C_{7a}$, $N_1$—$C_2$ and $C_{3a}$—$C_{7a}$ bonds and a decrease in BCPs of the $C_2$—$C_3$ and $C_3$—$C_{3a}$ bonds. The $N_1$—$C_2$, $C_2$—$C_3$ and $C_3$—$C_{3a}$ bonds showed a significant increase of the ellipticity.

A lengthening of the $N_1$—$C_2$, $C_2$—$C_3$ and $C_3$—$C_{3a}$ bonds and a slight shortening of the $N_1$—$C_{7a}$ and $C_{3a}$—$C_{7a}$ bonds were found in TRA. As expected, the $\rho_b$ values showed a decrease in BCPs of the $N_1$—$C_2$, $C_2$—$C_3$ and $C_3$—$C_{3a}$ bonds and an increase in BCPs of the $N_1$—$C_{7a}$ and $C_{3a}$—$C_{7a}$ bonds. The $N_1$—$C_2$, $C_2$—$C_3$, $C_3$—$C_{3a}$ bonds

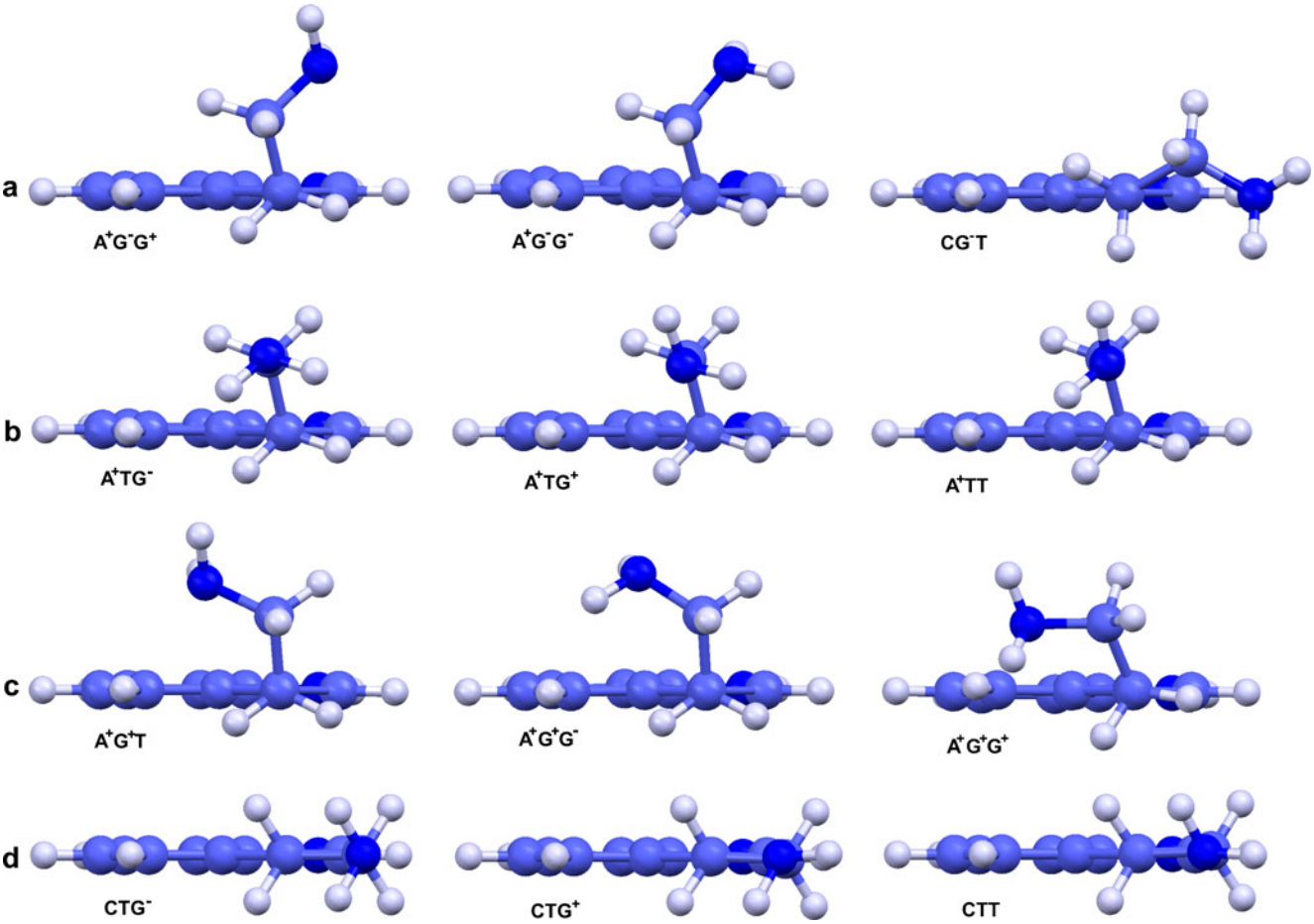


**Fig. 2** Twelve most stable conformers of TRA. According to IUPAC recommendations the first letter characterizes the orientation of the $C_9$ atom relative to the central $C_3$—$C_8$ bond, the second letter describes the $C_3$—$C_8$—$C_9$—$N_{10}$ angle, and the third letter specifies the orientation of the $H_a$ relative to the central $C_9$—$N_{10}$

**Table 1** Relevant internal coordinates of lowest energy conformers of TRA calculated at the B3LYP/6-31+G** level of theory[a,b]

| Conformers | ΔE | Dihedral angles | | |
|---|---|---|---|---|
| | | $\delta_1$ | $\delta_2$ | $\delta_3$ |
| $A^+G^-G^+$ | 0 | 103.2 | −64.0 | 64.5 |
| $A^+G^-G^-$ | 0.23 | 104.3 | −62.8 | −61.1 |
| $A^+TG^-$ | 0.54 | 102.4 | 178.5 | −60.6 |
| $A^+G^+T$ | 0.54 | 95.0 | 65.6 | 174.6 |
| $A^+TG^+$ | 0.68 | 103.7 | 176.5 | 66.6 |
| $A^+TT$ | 0.69 | 104.0 | −179.5 | 174.1 |
| $A^+G^+G^-$ | 0.81 | 86.6 | 61.8 | −57.6 |
| $CTG^-$ | 1.11 | 0.0 | 180.0 | −59.6 |
| $CG^-T$ | 1.07 | 30.1 | −66.5 | 179.3 |
| $CTG^+$ | 1.37 | −2.3 | 179.0 | 66.3 |
| CTT | 1.37 | 2.3 | −179.0 | 174.5 |
| $A^+G^+G^+$ | 2.55 | 114.6 | 83.3 | 74.4 |

[a] ΔE are expressed in kcal $mol^{-1}$ and dihedral angles in degrees

[b] Only *Re* isomers are shown

showed a significant increase of the ellipticity. Ellipticity measures the extent to which density is preferentially accumulated in a given plane containing the bond path. If $\lambda_1=\lambda_2$, then $\varepsilon=0$, and the bond is cylindrically symmetric, e.g., a C—C single bond in ethane, and a triple bond in acetylene. From the differences found with respect to Indole, our results showed that the acetyl and aminoethyl moiety induced a slight loss of symmetry in the electronic distribution of nearest bonds. An electron-releasing effect transmitted toward the closer bonds ($C_2$—$C_3$ and $C_3$—$C_{3a}$) is expected in both cases. However, the effect of the aminoethyl substituent seems to be higher over $N_1$—$C_2$ bond (nearest to the pyrrolic nitrogen). These observations can be interpreted as higher hyperconjugation effects in ring A of IAA and TRA.

Both in IAA and in TRA, was observed that the substituents produced slight changes on ring B. According to topological properties, both in IAA and in TRA, the values of ε in CPs of the $C_4$—$C_5$ and $C_6$—$C_7$ bonds were around 0.237 and the values of ε in CPs of the $C_{3a}$—$C_4$, $C_5$—$C_6$ and $C_7$—$C_{7a}$ bonds were around 0.196. Taking into

**Table 2** Bond lengths and topological properties at bond critical points (BCPs) for Indole, IAA and TRA calculated at the B3LYP/6-311++G** level of theory[a,b]

| x | | Bond length | | | $\rho_b$ | | | ε | | |
|---|---|---|---|---|---|---|---|---|---|---|
| | Bond | Indole | $\%\Delta x_{IAA}$ | $\%\Delta x_{TRA}$ | Indole | $\%\Delta x_{IAA}$ | $\%\Delta x_{TRA}$ | Indole | $\%\Delta x_{IAA}$ | $\%\Delta x_{TRA}$ |
| Ring A | $N_1$—$C_{7a}$ | 1.382 | −0.04 | −0.14 | 0.298 | 0.13 | 0.47 | 0.120 | −0.82 | −0.58 |
| | $N_1$—$C_2$ | 1.384 | −0.26 | 0.11 | 0.296 | 0.45 | −0.35 | 0.144 | 2.99 | 5.56 |
| | $C_2$—$C_3$ | 1.372 | 0.14 | 0.28 | 0.320 | −0.19 | −0.38 | 0.331 | 6.67 | 4.10 |
| | $C_3$—$C_{3a}$ | 1.439 | 0.34 | 0.49 | 0.282 | −0.60 | −0.96 | 0.166 | 6.75 | 2.68 |
| | $C_{3a}$—$C_{7a}$ | 1.425 | −0.15 | −0.08 | 0.298 | 0.38 | 0.20 | 0.201 | 0.84 | −0.09 |
| | $N_1$—H | 1.007 | 0.00 | −0.02 | 0.340 | −0.02 | 0.01 | 0.050 | 0.23 | 1.69 |
| | $C_2$—H | 1.081 | −0.02 | 0.06 | 0.284 | 0.14 | −0.20 | 0.041 | 0.41 | 6.89 |
| Ring B | $C_{3a}$—$C_4$ | 1.408 | −0.02 | 0.01 | 0.299 | −0.07 | −0.08 | 0.182 | 0.01 | 0.05 |
| | $C_4$—$C_5$ | 1.391 | 0.02 | 0.03 | 0.309 | −0.07 | −0.09 | 0.238 | −1.21 | −0.86 |
| | $C_5$—$C_6$ | 1.413 | −0.04 | −0.03 | 0.297 | 0.15 | 0.13 | 0.191 | 0.03 | 0.52 |
| | $C_6$—$C_7$ | 1.392 | −0.01 | −0.06 | 0.308 | 0.03 | 0.04 | 0.240 | −0.58 | −0.23 |
| | $C_7$—$C_{7a}$ | 1.401 | −0.05 | −0.02 | 0.303 | 0.16 | 0.13 | 0.215 | 0.05 | −0.04 |
| | $C_4$—H | 1.087 | −0.04 | −0.03 | 0.279 | 0.31 | 0.17 | 0.021 | −3.54 | −1.75 |
| | $C_5$—H | 1.086 | −0.01 | 0.00 | 0.280 | 0.09 | −0.02 | 0.025 | −1.01 | 1.68 |
| | $C_6$—H | 1.086 | −0.01 | 0.00 | 0.280 | 0.07 | −0.01 | 0.023 | −2.22 | −0.53 |
| | $C_7$—H | 1.087 | −0.02 | 0.00 | 0.278 | 0.06 | −0.01 | 0.026 | −0.82 | 0.12 |

[a] $\rho_b$, is expressed in a.u. and bond lengths in Å

[b] %Δ is the percentage difference relative to Indole for averaged values of eight conformers of IAA and for averaged values of 12 conformers of TRA

account these values of ellipticity and those corresponding to ethane, benzene and ethene considered as references and calculated at the same level of theory (0.000, 0.200 and 0.332, respectively), higher character of double bond was observed in $C_4$—$C_5$ and $C_6$—$C_7$ bonds than in $C_{3a}$—$C_4$, $C_5$—$C_6$ and $C_7$—$C_{7a}$ bonds. Interestingly, in Table 2 it can be seen that the bonds of higher (lower) ellipticity in Indole showed decrease (increase) of ε values in IAA and TRA. Therefore the changes introduced on ring B in IAA and TRA by the side chain indicated that in both cases there was a tendency to the equalization of the bond ellipticities (resonance effect).

Consequently, our results showed an increase of hyperconjugative and conjugative effects in the whole indole ring both in IAA as in TRA with respect to Indole and could be related to the higher antioxidant effectiveness in vitro of TRA [26, 27].

The AIM analysis allowed us to identify and characterize intramolecular hydrogen bonding (HB) interactions: a) $N_{10}\cdots$H—$C_2$ ($CG^-T$) and b) $N_{10}\cdots$H—$C_4$ ($A^+G^+G^+$). These H-bonds close six membered (in $CG^-T$), and seven-membered (in $A^+G^+G^+$) rings respectively and are accompanied by the appearance of ring critical points (RCPs), as required to fulfill the Poincaré-Hopf relationship [17]. Local topological properties calculated in the respective BCP and ring critical points (RCP) are displayed in Table 3. All these particular HBs were described by relatively low $\rho_b$ values, $\nabla^2\rho_b>0$, $|\lambda_1|/\lambda_3<1$ and $G_b/\rho_b<1$. They were classified as closed shell interactions.

Although both conformers presented hydrogen bonding interactions of similar strength, in $CG^-T$ conformer this interaction was characterized by a high ellipticity. The ellipticity value also is a measure of the structure stability [17]. A higher value of ε indicates a BCP near to coalesce with the corresponding RCP, which signifies the breaking of the bond. Our results indicate a less stable HB in $CG^-T$ than in $A^+G^+G^+$.

## NBO analysis

The NBO analysis provides energies of hyperconjugative interactions from the second-order perturbation approach:

$$E^{(2)} = -n_i \frac{F_{ij}^2}{\varepsilon_j - \varepsilon_i}, \quad (2)$$

where $F_{ij}$ is the Fock matrix element between the $i$ and $j$ NBO orbitals, $\varepsilon_j$ and $\varepsilon_i$ are the energies of $i$ and $j$ NBOs, and $n_i$ is the population of the donor $i$ orbital. Thus two main terms controlling the magnitude of a $i \rightarrow j$ hyperconjugative interaction namely: the difference in energy

**Table 3** Topological properties at bond critical points (BCPs) for hydrogen bonds in conformers of TRA calculated at the B3LYP/6-311++G** level of theory. Relevant topological properties at (3, +1) BCPs for the corresponding *pseudo*-rings are also reported[a]

| BCP | Conformers | H-bond | Distance | $\rho_b$ | $\nabla^2\rho_b$ | $\lambda_1$ | $\lambda_2$ | $\lambda_3$ | $\varepsilon$ | $G_b/\rho_b$ | $\lvert\lambda_1\rvert/\lambda_3$ |
|---|---|---|---|---|---|---|---|---|---|---|---|
| (3,-1) | $CG^-T$ | $H_2\cdots N_{10}$ | 2.560 | 0.011 | 0.036 | −0.010 | −0.008 | 0.054 | 0.199 | 0.678 | 0.183 |
| | $A^+G^+G^+$ | $H_4\cdots N_{10}$ | 2.561 | 0.011 | 0.030 | −0.010 | −0.009 | 0.049 | 0.072 | 0.603 | 0.201 |
| (3,+1) | $CG^-T$ | $H_2\cdots N_{10}$ | – | 0.009 | 0.043 | −0.005 | 0.012 | 0.036 | – | | |
| | $A^+G^+G^+$ | $H_4\cdots N_{10}$ | – | 0.005 | 0.022 | −0.002 | 0.009 | 0.015 | – | | |

[a] $\rho_b$, $\nabla^2\rho_b$, $G_b/\rho_b$, $\lambda_1$, $\lambda_2$, $\lambda_3$ are expressed in a.u. and distance in Å

between the interacting orbitals (the $\Delta E=\varepsilon_j - \varepsilon_i$ term) and the magnitude of the Fock matrix element, $F_{ij}$, which varies in parallel to the overlap matrix element, $S_{ij}$ [28].

An NBO analysis allowed us to investigate which orbital interactions are mainly involved in the stability of the observed conformers. Table 4 shows summations of second order stabilization energies ($E^{(2)}$) related to bonds of the side chain: $C_3$—$C_8$, $C_8$—$C_9$ , $C_9$—$N_{10}$ and the lone pair of nitrogen ($LP_{N10}$), which describe charge delocalization effects thus explaining the stability order of the described conformers. The orbital interactions which involve the $N_{10}$ lone pair were relevant ($LP_{N10}\rightarrow\sigma^*$); in fact in $A^+G^+G^-$, $CTG^-$, $CG^-T$, $CTG^-$, $CTG^+$, CTT and $A^+G^+G^+$ conformers were enough to explain the stability order. The summations of the second order stabilization energies involved several charge delocalizations. The charge transference in which the lone pair delocalizes toward a *trans* bonding orbital always was the relevant one. The higher values were found in $A^+G^+G^-$ and $CTG^-$ where the *trans* bonding orbital (acceptor orbital) corresponds to a C—C bond ($\sigma^*_{C—C}$). The remaining conformers showed lower values because the *trans* bonding orbital corresponds to a C—H bond ($\sigma^*_{C—H}$), thus showing C—C antibonding orbitals as better acceptor than C—H antibonding orbitals [28].

In $A^+TG^-$, $A^+G^+T$, $A^+TG^+$ and $A^+TT$ the consideration of transferences from $C_3$—$C_8$ and $C_8$—$C_9$ bonding orbitals were also needed to explain their stability order. Finally in $A^+G^-G^+$ and $A^+G^-G^-$ the transferences from $C_9$—$N_{10}$ bonding orbital were required thus showing how the better delocalization of electronic charge is related to higher stabilization of the structure.

To analyze in depth the stereoelectronic effects that operate in TRA we classified the conformers under study into four groups according to the position of the amino group relative to the indole ring: *gauche* on the pyrrole (group $G^-$), *gauche* on the phenyl (group $G^+$) or *anti* related to indole ring (groups T and T′), see Fig. 3.

The conformers belonging to the same group share a common configuration relative to the $C_8$—$C_9$ bond. For example the $A^+G^-G^+$, $A^+G^-G^-$ and $CG^-T$ conformers have in common the dihedral angle $\delta_2$ (clinal array), with the aminoethyl group oriented toward the pyrrole (Table 1).

Relevant NBO second-order stabilization energies for the group $G^-$, are shown in Table 5. The charge transferences related to the electronic delocalization between indole backbone and aminoethyl moiety are reported. Strongest charge delocalization in $A^+G^-G^+$ was found which explains their higher stability (see also Fig. 4a where the black squares represent the summation of relevant transferences inside each group, while the red circles correspond only to delocalization from $C_3$—$C_8$ bonding orbital toward a *trans* antibonding orbital). Moreover,

**Table 4** Summation of second-order stabilization energies, $E^{(2)}$, for relevant donors of TRA conformers calculated at the B3LYP/6-311++G** level of theory[a]

| Donor | $\Sigma E^{(2)}$ | | | | | | | | | | | |
|---|---|---|---|---|---|---|---|---|---|---|---|---|
| | $A^+G^-G^+$ | $A^+G^-G^-$ | $A^+TG^-$ | $A^+G^+T$ | $A^+TG^+$ | $A^+TT$ | $A^+G^+G^-$ | $CTG^-$ | $CG^-T$ | $CTG^+$ | CTT | $A^+G^+G^+$ |
| $LP_{N10}$ | 10.01 | 12.6 | 12.25 | 10.16 | 9.89 | 9.81 | 12.74 | 12.01 | 9.96 | 9.84 | 9.84 | 9.56 |
| $\sigma_{C3—C8}$ | 9.21 | 8.31 | 9.41 | 9.17 | 9.05 | 8.69 | | | | | | |
| $\sigma_{C8—C9}$ | 6.67 | 4.98 | 4.86 | 6.84 | 6.55 | 6.41 | | | | | | |
| $\Sigma$ | | | 26.52 | 26.17 | 25.49 | 24.91 | | | | | | |
| $\sigma_{C9—N10}$ | 1.19 | 0.88 | | | | | | | | | | |
| $\Sigma$ | 27.08 | 26.77 | | | | | | | | | | |

[a] All values are expressed in kcal $mol^{-1}$

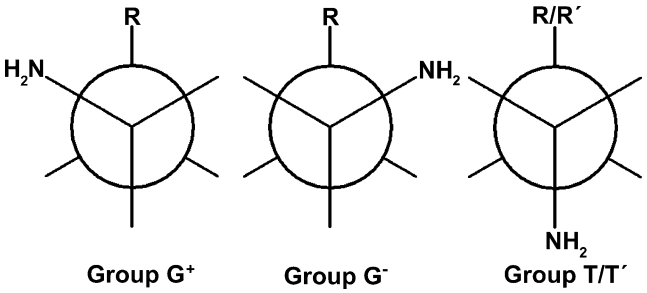


**Fig. 3** Scheme of groups $G^+$, $G^-$, T and T′ which ones differ in the dihedral angle $\delta_2$. R designates conformers with indole ring at right angles to the $C_8$—$C_9$ bond and R′ designates conformers with indole ring parallel to the $C_8$—$C_9$ bond

**Table 5** Second-order stabilization energies, $E^{(2)}$, calculated at the B3LYP/6-311++G** level of theory for donation transferences related to the group $G^{-a}$

| Donor | Acceptor | $E^{(2)}$ | | |
|---|---|---|---|---|
| | | $A^+G^-G^+$ | $A^+G^-G^-$ | $CG^-T$ |
| $LP_{N10}$ | $\sigma^*_{C2—H}$ | – | – | 0.86 |
| | $\sigma^*_{C8—C9}$ | 0.90 | 8.95 | 0.77 |
| | $\sigma^*_{C9—Ha}$ | 7.79 | 1.65 | 1.32 |
| | $\sigma^*_{C9—Hb}$ | 1.32 | 1.29 | 7.01 |
| $\sigma_{C3a—C3}$ | $\sigma^*_{C3—C8}$ | 1.71 | 1.36 | 1.71 |
| | $\sigma^*_{N1—C2}$ | 1.00 | 0.97 | 1.03 |
| $\sigma_{C2—C3}$ | $\sigma^*_{C3—C8}$ | 2.13 | 1.83 | 2.22 |
| $\pi_{C2—C3}$ | $\sigma^*_{C8—C9}$ | 3.69 | 3.67 | 0.69 |
| | $\sigma^*_{C8—Ha}$ | 2.15 | 2.24 | 1.16 |
| $\sigma_{C3a—C7a}$ | $\sigma^*_{C3—C8}$ | 5.11 | 5.03 | 5.09 |
| $\sigma_{C3—C8}$ | $\sigma^*_{C3a—C7a}$ | 1.61 | 1.56 | 1.61 |
| | $\sigma^*_{C2—C3}$ | 2.47 | 2.08 | 2.60 |
| | $\sigma^*_{C9—Hb}$ | 1.27 | 1.17 | 1.06 |
| $\sigma_{C8—C9}$ | $\sigma^*_{C2—C3}$ | 1.38 | 1.41 | – |
| | $\pi^*_{C2—C3}$ | 2.60 | 2.74 | 0.52 |
| | $\sigma^*_{N10—Hb}$ | 1.88 | – | – |
| $\sigma_{C9—N10}$ | $\sigma^*_{C8—Ha}$ | 1.19 | 0.88 | 1.12 |
| $\sigma_{C8—Ha}$ | $\sigma^*_{C2—C3}$ | 3.61 | 3.54 | 4.87 |
| | $\pi^*_{C2—C3}$ | 2.46 | 2.54 | 1.29 |
| $\sigma_{C8—Hb}$ | $\sigma^*_{C3—C8}$ | 5.42 | 5.48 | – |
| $\sigma_{C9—Ha}$ | $\sigma^*_{C8—Hb}$ | 2.70 | 2.81 | 2.89 |
| $\sigma_{C9—Hb}$ | $\sigma^*_{N10—Ha}$ | 3.19 | – | – |
| | $\sigma^*_{N10—Hb}$ | – | 3.33 | – |
| $\sigma_{N10—Ha}$ | $\sigma^*_{C8—C9}$ | – | – | 2.81 |
| | $\sigma^*_{C9—Ha}$ | – | 2.34 | – |
| | $\sigma^*_{C8—Hb}$ | 2.21 | – | – |
| $\sigma_{N10—Hb}$ | $\sigma^*_{C8—C9}$ | 2.85 | – | – |
| | $\sigma^*_{C9—Ha}$ | – | – | 2.27 |
| | $\sigma^*_{C9—Hb}$ | – | 2.32 | – |
| | Σ | 60.64 | 59.19 | 42.90 |

[a] All values are expressed in kcal $mol^{-1}$

similar trends were found in the other groups ($G^+$, T and T′) thus explaining the stability order in each case (Table S2a, S2b and S2c and Fig. 4b, c and d).

Moreover, we found that specific charge delocalization from $C_3$—$C_8$ bonding orbital toward the side chain plays a relevant role in the stabilization of the structures inside each group. In fact, it is interesting to note for example that in group $G^-$ the $\sigma_{C3—C8} \rightarrow \sigma^*_{C9—Hb}$ transference is related to the trend found in Table 5 (see red circles in Fig. 4a). The $E^{(2)}$ values were proportional to $F_{ij}$ term (0.032, 0.031 and 0.029 a.u. in $A^+G^-G^+$, $A^+G^-G^-$ and $CG^-T$, respectively). These delocalization were associated to $\delta_{C3—C8—C9—Hb}$ dihedral angle (177.9°, 175.2° and 168.7° for $A^+G^-G^+$, $A^+G^-G^-$ and $CG^-T$, respectively) thus allowing us to propose an increased orbital overlap due to the increase in $\delta_{C3—C8—C9—Hb}$ dihedral angle (better overlapping when the bonds are antiperiplanar to each other). Similarly, we found that in group $G^+$ the $\sigma_{C3—C8} \rightarrow \sigma^*_{C9—Ha}$ transference plays a similar role (see red circles in Fig. 4b). We also found that in T and T′groups the $\sigma_{C3—C8} \rightarrow \sigma^*_{C9—N10}$ transferences explain the stability order (see circles in Fig. 4c and d).

Finally we found higher variations of molecular energies for conformers inside *clinal* groups (where the relevant charge transfers went toward $C_9$—H bonds). In *anti* groups the different conformers differed only slightly in energy (where the relevant charge transfers go toward $C_9$—$N_{10}$ bonds). These results indicated a higher sensitivity to conformational changes in $C_9$—$H_a$ and $C_9$—$H_b$ bonds than in $C_9$—$N_{10}$ bond.

## AIM/NBO study of molecular electrostatic potential electrostatic potential

The molecular electrostatic potential ($V$(r)) have been used extensively for interpreting and predicting the reactive behavior of a wide variety of chemical systems in both electrophilic and nucleophilic reactions, in the study of hydrogen bonding interactions and in biological recognition processes [29–32] and can be determined experimentally by diffraction techniques or obtained by computational methods [29].

This paper uses the procedure proposed by Politzer et al. [29] for predicting sites targeted for electrophilic attack in the regions of negative $V$(r) values, together with some NBO and AIM results in light of the complementarities of these different theoretical tools.

The nitrogen atoms are sites that exhibit the highest concentration of charge (Fig. 5). The $N_{10}$ has the highest negative $V$(r) (−59.90 kcal $mol^{-1}$), meanwhile the $N_1$ has a lower negative $V$(r) (−41.01 kcal $mol^{-1}$). At $C_5$ we also found negative electrostatic potential (−28.42 kcal $mol^{-1}$). The latter, indicates activation to electrophilic attack also at position 5 in ring B of TRA. These findings could be related to the antioxidant properties of indole derivatives.

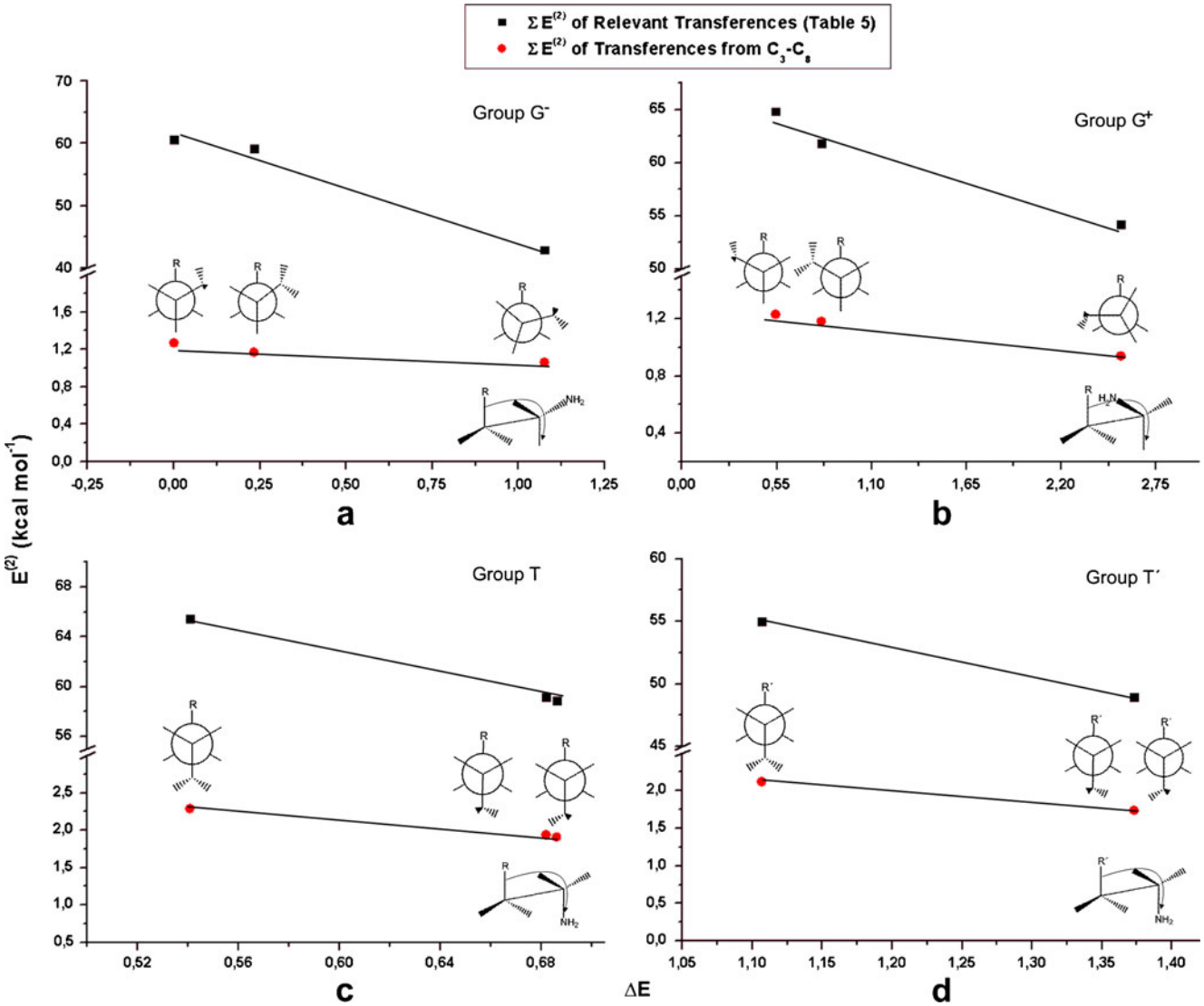


**Fig. 4** Second order energies for relevant NBO stabilization energies for the groups $G^-$ (**a**), $G^+$ (**b**), T (**c**) and T′ (**d**) *vs.* relative conformational energies (black squares). Second order energies for $\sigma_{C3—C8} \rightarrow \sigma^*_{C9—Ha/\ Hb/N10}$ transferences *vs.* relative conformational energies (red circles)

In previous works [15, 33, 34] we showed that coordinated analysis of NBO and AIM results allowed to rationalize new aspects of the potential created in the space around a molecule. Following the same line of reasoning

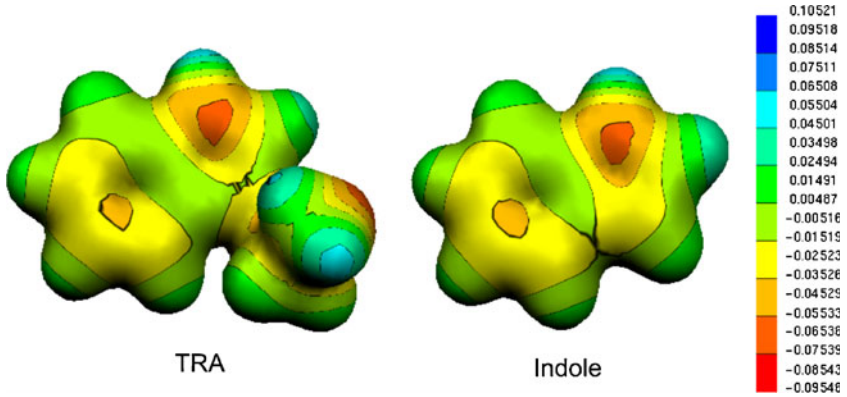


**Fig. 5** MEPs for $A^+G^-G^+$ conformer of TRA and Indole. Values in a.u

we found in TRA that the negative $V$(r) values on nitrogen atoms that comprise a hydrogen bond (atom of the acceptor moiety) become less negative (higher) than the $V$(r) values of those nitrogen atoms that do not comprise it. The positive $V$(r) values on hydrogen atoms of the N···H hydrogen bridge (belonging to the donor C—H moiety) become less positive (lower) than the other hydrogen atoms of the benzene ring (Fig. 6). In fact, N···H intramolecular weak interactions, and their marked directionality were characterized by the asymmetrization of the $V$(r) distribution on hydrogen atoms of the bridge, which is clearly defined by the neighbor nitrogen (Fig. 6). Thus, through an AIM/NBO point of view of the MEPs, the analysis of intramolecular N···H hydrogen bonds can be enriched, showing a $V$(r) value increase on the atom that belongs to the acceptor moiety, while a $V$(r) value decrease on that of the donor moiety, in agreement with the electrostatic potential complementarily between positive regions of H-donor groups and negative regions of the H-acceptor atom found in intermolecular H-bonds [35]. These features were reported previously in other systems for O···H hydrogen bonds [15].

$A^+G^+G^+$ conformer, which is the more destabilized, showed negative potential on a higher extended area on benzene ring (Fig. 7 ($A^+G^+G^+$)) which is near the negative region on $N_{10}$. Therefore, this feature of MEP is an indicator of the instability of this conformer with respect to the others and justifies why this conformer was not observed experimentally. In fact, in this conformer the nitrogen lone pair points in toward the indole π-cloud, which destabilizes these minima with respect to the others [6]. Figure 7 also allows us to describe the changes on negative $V$(r) values on $N_1$. Interestingly, through NBO analysis we found that the difference between charge transfers toward the $N_1$—H bond and reverse charge transfers that remove charge from the $N_1$—H bond are related to the extension of the region of higher negative $V$(r) value on $N_1$ (4.88, 4.87 and 4.99 kcal mol$^{-1}$ in $A^+G^-G^+$, $A^+G^-G^-$ and $CG^-T$ respectively and 4.89, 4.88 and 5.02 kcal mol$^{-1}$ in $A^+G^+T$, $A^+G^+G^-$ and $A^+G^+G^+$ respectively). In fact, the larger the net transferred charge to $N_1$ region, the larger the region of higher negative value of $V$(r) in it. In Fig. 5 similar features both in Indole and $A^+G^-G^+$ conformer of TRA can be observed on $N_1$ and in fact the net transferred charge was similar in both cases (4.88 kcal mol$^{-1}$).

MEPs of the conformers of the group T ($A^+TG^-$, $A^+TG^+$ and $A^+TT$) are shown in Fig. 8. Changes on negative $V$(r) values on $N_{10}$ can be observed. In fact, the negative values of $V$(r) on $N_{10}$ in $A^+TG^-$ conformer (−41.01 kcal mol$^{-1}$) become less negative (higher) than $V$(r) on $N_{10}$ in the other conformers (≈−53.61 kcal mol$^{-1}$). Interestingly, a higher hyperconjugative delocalization from the $LP_{N10}$ was found (see Table 4). Similar behavior of MEPs was reported previously in IAA in connection with the donor role of C—H bonds [35]. The higher donor ability of $LP_{N10}$ in $A^+TG^-$ was found for $LP_{N10} \rightarrow \sigma^*_{C8—C9}$ transfer which can be related to the *trans* orientation of $LP_{N10}$ with respect to $C_8$—$C_9$ bond thus improving the electron delocalization. In $A^+TG^+$ and $A^+TT$ the acceptor orbitals corresponded to C—H bonds ($\sigma^*_{C—H}$), thus showing C—C antibonding orbital is a better acceptor than C—H antibonding orbital. A similar behavior was observed for $A^+G^-G^-$ in group $G^-$ and for $CTG^-$ in group T′ (Figs. S1 and S2, respectively) thus showing that, given a similar electric environment, the better $LP_{N10}$ donor role is associated to a less negative $V$(r) on $N_{10}$ .

## Conclusions

The study of conformational space of TRA was performed in vacuum thus describing intrinsic properties, deepening in the analysis of the geometric and electronic properties and how the conformational flexibility of the side chain introduces electronic changes in the molecule. The results reported contribute to the understanding of the structure, stability, and reactivity of TRA and others indole deriva-

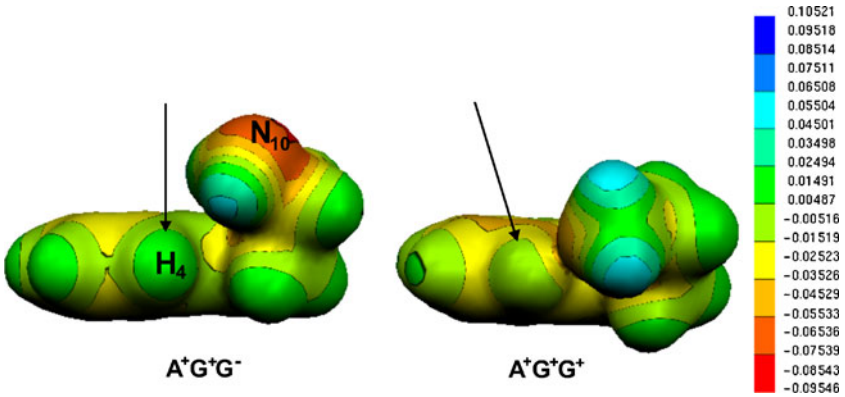


**Fig. 6** MEPs for $A^+G^+G^-$ and $A^+G^+G^+$ conformers of TRA. With *vertical line* a hydrogen atom not involved in intramolecular H-bond is indicated and with *oblique line* a hydrogen atom involved in intramolecular H-bond is shown. Values in a.u

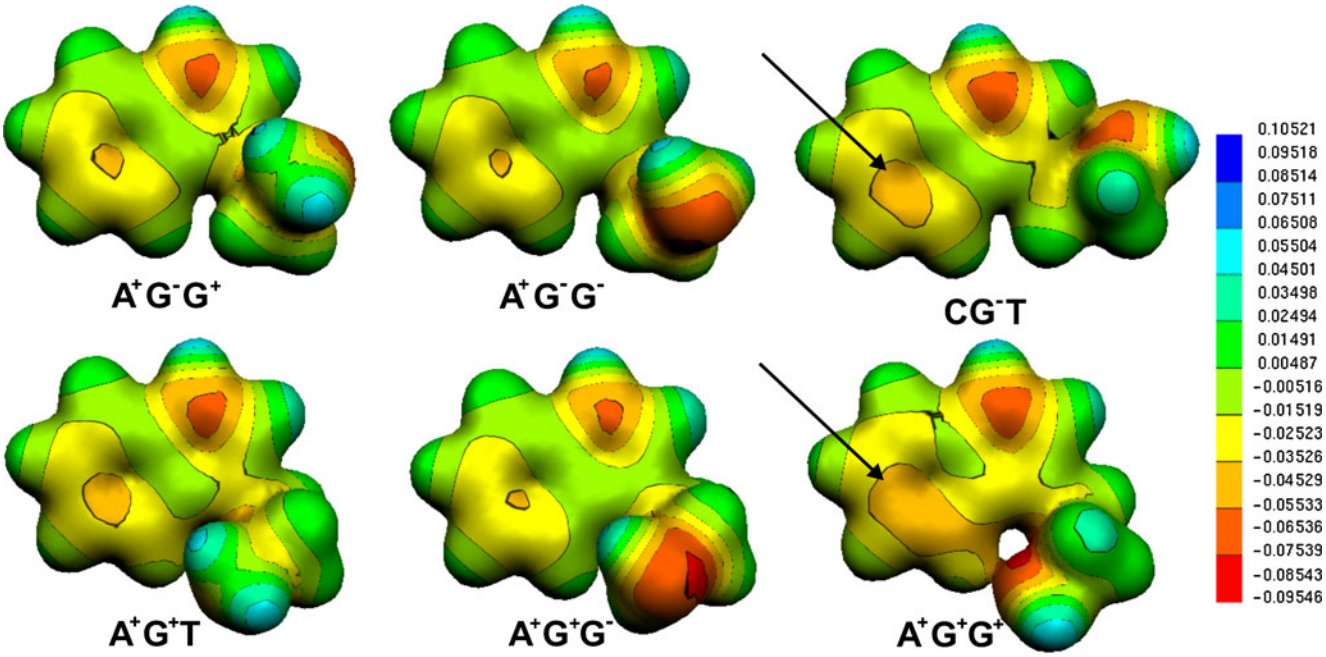


**Fig. 7** MEPs for $A^+G^-G^+$, $A^+G^-G^-$, $CG^-T$, $A^+G^+T$, $A^+G^+G^-$ and $A^+G^+G^+$ conformers of TRA. *Oblique lines* indicate the changes at $C_5$. Values in a.u

tives. Twenty one lowest energy conformers with symmetry $C_1$ were characterized and thoroughly analyzed. The first seven more stable conformers were previously observed experimentally and we described also four conformers unobserved experimentally which present a relative population less than 6%.

The NBO analysis showed the occurrence of orbital interactions (mostly hiperconjugation) which play a relevant role to stabilize the conformers. The orbital interactions which involve the $N_{10}$ lone pair were relevant ($LP_{N10} \rightarrow \sigma^*$).

To analyze in depth the stereoelectronic effects that operate in TRA we classified the conformers under study into four groups according to the position of the amino group relative to the indole ring: *gauche* on the pyrrole (group $G^-$), *gauche* on the phenyl (group $G^+$) or *anti* related to indole ring (groups T and T′). We found that specific charge delocalizations from $C_3$—$C_8$ bonding orbital toward the side chain play a relevant role in the stabilization of the structures inside each group. The structural factors of molecular geometry which explain the better charge delocalization effects were found and described.

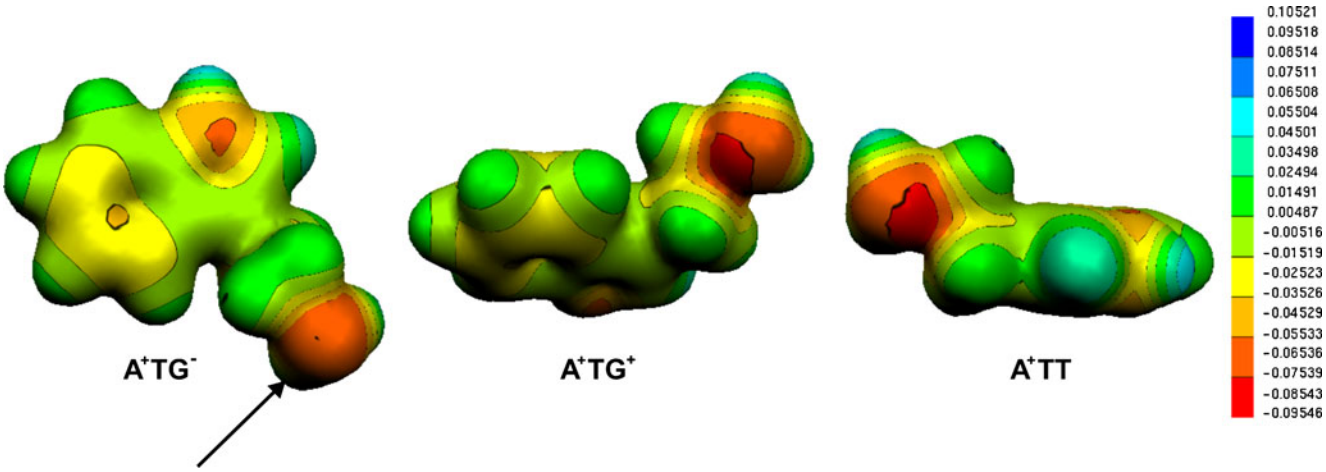


**Fig. 8** MEPs for $A^+TG^-$, $A^+TG^+$ and $A^+TT$ conformers of TRA. Changes on negative $V(r)$ values on $N_{10}$ can be observed: the negative values of $V(r)$ on $N_{10}$ in $A^+TG^-$ conformer (*oblique line*) become less negative (higher) than $V(r)$ on $N_{10}$ in the other conformers. Values in a.u

Through the MEPs the sites targeted for electrophilic attack were predicted and analyzed. Moreover, the coordinated analysis of MEPs and NBO and AIM results for conformers under study, also allowed us to rationalize some aspect of the potential created in the space around a molecule. In fact, we showed features of MEP as an indicator of:

- The N···H intramolecular weak interactions, and their marked directionality.
- The instability of $A^+G^+G^+$ conformer with respect to the others.
- The higher charge tranferences toward $N_1$ region.
- The larger donor ability of lone pairs of $N_{10}$ in hyperconjugative transferences.

Through an AIM analysis we characterized the expected intramolecular interactions as covalent bonds and also we identified and characterized the intramolecular hydrogen bonding interactions $N_{10}\cdots H—C_2$ and $N_{10}\cdots H—C_4$ in $CG^-T$ and $A^+G^+G^+$ respectively.

The changes in geometric parameters and topological properties introduced in the indole ring by substitution at position 3 with acetyl (IAA) and aminoethyl (TRA) moieties were quantified. It was noted that the two rings (benzenic as well as pyrrolic) showed changes in bond lengths and topological properties. From the differences found with respect to Indole, our results showed that the acetyl and aminoethyl moieties produce an increase in the effectiveness of hypercongugative and conjugative interactions. The higher charge delocalization effects found in IAA and TRA could be related to an improved stabilization of the cation radical or the radical generated in the free radical scavenging process.

The reported study of the conformational space in vacuum to describe intrinsic properties is a relevant first step in the description of the reactivity of TRA in aqueous solution and in the study of their IR and Raman spectrum which are in progress in our laboratory.

**Acknowledgments** Thanks are due to Agencia de Promoción Científica y Tecnológica Argentina (MINCYT), CONICET and Universidad Nacional de La Plata (Argentina) for financial support. A.H.J. is a Member of the Scientific Research Career (CIC, Provincia de Buenos Aires). A.A.V. is a Research Member of the National Research Council of Argentina (CONICET). M.C.P.S. acknowledges a fellowship (IP-PRH N0 54) from Agencia de Promoción Científica y Tecnológica Argentina and Universidad de la Cuenca del Plata (Corrientes, Argentina) and R.M.L. acknowledges Universidad de la Cuenca del Plata for facilities provided during the course of this work.

## References

1. Khan MTH (2007) Bioactive heterocycles V. Springer, Berlin, pp 145–154
2. Bozkaya P, Dogan B, Suzen S, Nebioglu D, Ozkan SA (2006) Determination and investigation of electrochemical behaviour of 2-phenylindole derivatives: Discussion on possible mechanistic pathways. Can J Anal Sci Spectrosc 51:125–139
3. Kruk I, Aboul-Enein HY, Michalska T, Lichszteld K, Kubasik-Kladna K, Olgen S (2007) In vitro scavenging activity for reactive oxygen species by N-substituted indole-2-carboxylic acid esters. J Lumin 22:379–386
4. Shirinzadeh H, Eren B, Gurer-Orhan H, Suzen S, Özden S (2010) Novel Indole-Based Analogs of Melatonin: Synthesis and in vitro Antioxidant Activity Studies. Molecules 15:2187–2202
5. Poeggeler B, Thuermann S, Dose A, Schoenke M, Burkhardt S, Hardeland R (2002) Melatonin's unique radical scavenging properties - roles of its functional substituents as revealed by a comparison with its structural analogs. J Pineal Res 33:20–30
6. Clarkson JR, Dian BC, Moriggi L, DeFusco A, McCarthy V, Jordan KD, Zwier TS (2005) Direct measurement of the energy thresholds to conformational isomerization in tryptamine: Experiment and theory. J Chem Phys 122: 214311-1-15
7. Park YD, Rizzo TR, Peteanu LA, Levy DH (1986) Electronic spectroscopy of tryptophan analogs in supersonic jets: 3-Indole acetic acid, 3-indole propionic acid, tryptamine, and N-acetyl tryptophan ethyl ester. J Chem Phys 84:6539–6549
8. Philips LA, Levy DH (1988) Rotationally resolved electronic spectroscopy of tryptamine conformers in a supersonic jet. J Chem Phys 89:85–90
9. Wu Y, Levy DH (1989) Determination of the geometry of deuterated tryptamine by rotationally resolved electronic spectroscopy. J Chem Phys 91:5278–5284
10. Connell LL, Corcoran TC, Joireman PW, Felker PM (1990) Conformational analysis of jetcooled tryptophan analogs by rotational coherence spectroscopy. Chem Phys Lett 166:510–516
11. Sipior J, Sulkes M (1993) Conformational analysis of jet cooled tryptophan analogs by molecular mechanics: Comparison with experiment. J Chem Phys 98:9389–9399
12. Carney JR, Zwier TS (2000) The infrared and ultraviolet spectra of individual conformational isomers of biomolecules: Tryptamine. J Phys Chem A 104:8677–8688
13. Carney JR, Zwier TS (2001) Conformatinal flexibility in small biomolecules: tryptamine and 3-indole-propionic acid. Chem Phys Lett 341:77–85
14. Böhm M, Brause R, Jacoby C, Schmitt M (2009) Conformational relaxation paths in tryptamine. J Phys Chem A 113:448–455, and references cited therein
15. Pérez Schmit MC, Jubert A, Vitale A, Lobayan RM (2010) Electronic structure and conformational properties of *1H*-indole-3-acetic acid. J Mol Model 17:1227–1239
16. Lobayan RM, Pérez Schmit MC, Jubert A, Vitale A (2010) Theoretical studies and vibrational spectra of *1H*-indole-3-acetic acid. Exploratory conformational analysis of dimeric species. J Mol Model 17:1381–1392
17. Bader RFW (1995) Atoms in molecules. A quantum theory. Oxford University Press, Oxford
18. Popelier P (2000) Atoms in molecules. An introduction. Prentice Hall
19. Glendening ED, Reed AE, Carpenter JE, Weinhold F NBO 3.1 (2003) Program as implemented in the Gaussian 03 package
20. HyperChem Release 7.5, Hypercube Inc, USA
21. Frisch MJ, Trucks GW, Schlegel HB, Scuseria GE, Robb MA, Cheeseman JR, Montgomery JA, Vreven T, Kudin KN, Burant JC, Millam JM, Iyengar SS, Tomasi J, Barone V, Mennucci B, Cossi M, Scalmani G, Rega N, Petersson GA, Nakatsuji H, Hada M, Ehara M, Toyota K, Fukuda R, Hasegawa J, Ishida M, Nakajima T, Honda Y, Kitao O, Nakai H, Klene M, Li X, Knox JE, Hratchian HP, Cross JB, Adamo C, Jaramillo J, Gomperts R, Stratmann RE, Yazyev O, Austin AJ, Cammi R, Pomelli C,

Ochterski JW, Ayala PY, Morokuma K, Voth GA, Salvador P, Dannenberg JJ, Zakrzewski VG, Dapprich S, Daniels AD, Strain MC, Farkas O, Malick DK, Rabuck AD, Raghavachari K, Foresman JB, Ortiz JV, Cui Q, Baboul AG, Clifford S, Cioslowski J, Stefanov BB, Liu G, Liashenko A, Piskorz P, Komaromi I, Martin RL, Fox DJ, Keith T, Al-Laham MA, Peng CY, Nanayakkara A, Challacombe M, Gill PMW, Johnson B, Chen W, Wong MW, Gonzalez C, Pople JA (2003) Gaussian03, Revision B.02. Gaussian Inc, Pittsburgh

22. Becke AD (1993) Density-functional thermochemistry. III. The role of exact exchange. J Chem Phys 98:5648–5652
23. Lee C, Yang W, Parr RG (1988) Development of the Colle-Salvetti correlation energy formula into a functional of the electron density. Phys Rev B 37:785–789
24. Flúrkiger P, Lúthi HP, Portmann S, Weber J (2000) MOLEKEL 4.0. Swiss Center for Scientific Computing, Manno
25. Biegler-Köning FW, Bader RFW, Tang TH (1982) Calculation of the average properties of atoms in molecules. II. J Comput Chem 3:317–328
26. Stetinova V, Smetanova L, Grossmann V, Anzenbacher (2002) In vitro and In vivo Assessment of antioxidant activity of melatonin and related indole derivates. Gen Physiol Biophys 21:153–162
27. Estevão MS, Carvalho LC, Ferreira LM, Fernandes E, Marques MMB (2011) Analysis of the antioxidant activity of an indole library: cyclic voltammetry versus ROS scavenging activity. Tetrahedron Lett 52:101–106
28. Alabugin IV, Zeidan TA (2002) Stereoelectronic effects and general trends in hyperconjugative acceptor ability of σ bonds. J Am Chem Soc 124:3175–3185
29. Politzer P, Truhlar DG (eds) (1981) Chemical applications of atomic and molecular electrostatic potentials. Plenum, NY
30. Politzer P, Murray JS (1991) Theoretical biochemistry and molecular biophysics: a comprehensive survey, vol 2. In: Beveridge DL, Lavery R (eds) Protein. Adenine, Schenectady, pp 165–191
31. Politzer P, Murray J, Concha MC (2002) The complementary roles of molecular surface electrostatic potentials and average local ionization energies with respect to electrophilic processes. Int J Quantum Chem 88:19–27
32. Roy DK, Balanarayan P, Gadre SR (2009) Signatures of molecular recognition from the topography of electrostatic potential. J Chem Sci 121:815–821
33. Lobayan RM, Jubert AH, Pomilio AB (2009) Conformational and electronic (AIM/NBO) study of unsubstituted A-type dimeric Proanthocyanidin. J Mol Model 15:537–550
34. Bentz E, Jubert AH, Pomilio AB, Lobayan RM (2010) Theoretical study of Z isomers of A-type dimeric proanthocyanidins substituted with R=H, OH and OCH3. Stability and reactivity properties. J Mol Model. doi:10.1007/s00894-010-0682-z
35. Pacios LF (2006) Chapter 3: changes of electron properties in the formation of hydrogen bonds. In: Grabowski SJ (ed) Hydrogen bonding-new insights. Springer, Berlin